Research article

Ji Huang, Lan Jiang*, Xiaowei Li, Andong Wang, Zhi Wang, Qingsong Wang, Jie Hu, Liangti Qu, Tianhong Cui and Yongfeng Lu

Fabrication of highly homogeneous and controllable nanogratings on silicon via chemical etching-assisted femtosecond laser modification

https://doi.org/10.1515/nanoph-2019-0056
Received February 21, 2019; revised March 21, 2019; accepted March 22, 2019

Abstract: Femtosecond laser direct writing is widely exploited in surface periodic structures processing. However, this technique still faces challenges in obtaining high surface homogeneity and flexible morphology controllability. In this study, a flexible and efficient approach has been proposed to fabricate highly homogeneous and controllable nanogratings on silicon via chemical etching-assisted femtosecond laser modification. By precisely manipulating the laser-material interaction process, alternating amorphous-crystalline nanofringes are generated when employing femtosecond laser scanning over a Si sample, with almost no material removal. Following auxiliary chemical etching, highly homogeneous nanograting structures are obtained, and the morphology of the nanogratings can be flexibly managed through precisely controlling the duration of the etching process. Complex cross-scale patterns with remarkable structural colors that are visible under indoor light illumination are readily achieved on the sample surfaces exploiting our method. In addition, compared with traditional methods for laser-induced periodic surface structures, the fabrication efficiency is considerably improved. Our processing procedure offers potential applications in the fields of optics, nanoelectronics, and mechatronics.

Keywords: femtosecond laser; chemical etching; nanograting structures; highly homogeneous; highly controllable.

1 Introduction

Photolithography provides a common method for processing grating structures [1]. However, the use of photoresist makes the process complicated. Besides, it requires expensive and custom apparatus to produce the master images. Focused ion beam milling or electron beam lithography could also be utilized to fabricate nanogratings [2–4]. Nevertheless, these nanofabrication techniques often call for complex setups and equipment, and it takes a relatively long time to finish the process [5]. Laser-induced periodic surface structure (LIPSS), first discovered on a semiconductor surface by Birnbaum in 1965 [6], provides a powerful contactless technique for the preparation of nanogratings on samples surface. For decades, plenty of works have been reported to explain the formation mechanism of LIPSS, and a widely accepted definition is the interference between the incident laser beam and surface plasmon polaritons (SPP), which induces local ablation of the material and ultimately forms LIPSS [7–10]. The effects of the laser parameters on the morphology of LIPSS have also been widely studied. Jiang et al. reported the abnormal enhancement ablation characteristics with polarization-dependent sensitivity [11]. Bonse and Krüger experimentally and theoretically studied the effect of pulse number on the formation of LIPSS [12]. Moreover, LIPSS has found broad promising applications, such as colorization [13, 14], waveguides [15], solar cells [16], water-repellent surfaces [17, 18], biological devices [19], and surface-enhanced Raman scattering [20].

***Corresponding author: Lan Jiang,** Laser Micro/Nano Fabrication Laboratory, School of Mechanical Engineering, Beijing Institute of Technology, Beijing 100081, China, e-mail: jianglan@bit.edu.cn. https://orcid.org/0000-0003-0488-1987
Ji Huang, Xiaowei Li, Andong Wang, Zhi Wang, Qingsong Wang and Jie Hu: Laser Micro/Nano Fabrication Laboratory, School of Mechanical Engineering, Beijing Institute of Technology, Beijing 100081, China
Liangti Qu: Department of Mechanical Engineering, Tsinghua University, Beijing 100084, P.R. China; and School of Chemistry and Chemical Engineering, Beijing Institute of Technology, Beijing 100081, P.R. China
Tianhong Cui: Department of Mechanical Engineering, University of Minnesota, Minneapolis, MN, 55455, USA
Yongfeng Lu: Department of Electrical and Computer Engineering, University of Nebraska-Lincoln, Lincoln, NE 68588-0511, USA

However, LIPSS always suffers from high surface nonhomogeneity, which is unfavorable for the applications in the field of optics, etc. [21]. In traditional LIPSS technology, high laser power is necessary to generate the structures through material ablation which often co-occurs with the formation of a lot of debris and surface defects, resulting in a significant nonhomogeneity of the consequent structures. In contrast, femtosecond laser irradiation below ablation threshold is capable of inducing crystalline-Si surface to melt and rapidly solidify into the amorphous phase [22–24]. In addition, by means of precisely adjusting the femtosecond laser parameters, laser fluence and effective pulse number, alternating amorphous-crystalline nanofringes can be created on Si sample surface via femtosecond laser-induced self-assembly processes. Unlike conventional LIPSS, the formation of amorphous-crystalline nanofringes is mainly accompanied by phase changing of crystalline Si, with almost no material removal [25]. Thus, the regularity of the Si nanofringes fabricated by femtosecond laser modification is higher. Notably, femtosecond laser-induced amorphization of monocrystalline silicon is deemed to change the average dangling bond density of the silicon atoms, which is a critical factor in determining the etching rate of silicon during subsequent chemical etching [26].

Nowadays, the selective removal of transparent materials or semiconductors by wet chemical etching has been extensively examined, and a wide range of applications is put forward in various fields, such as optics [27], solar cells [28], nanoenergy [29, 30], etc. The combination of laser direct writing and chemical etching has been reported to better control micro/nano structures [31–34]. In this paper, a flexible and efficient approach has been proposed to fabricate nanogratings on silicon with high homogeneity and controllability via chemical etching-assisted femtosecond laser modification. This method involves the construction of amorphous-crystalline nanofringes where crystalline silicon is transformed to amorphous silicon by precisely managing the femtosecond laser-material interaction process in the first step. Compared with the conventional methods, the fabrication efficiency can be enhanced by approximately 2–3 times, as the laser fluence and effective pulse number required for the formation of the modified nanofringes are much lower than those for the traditional LIPSS. Afterwards, highly homogeneous nanograting structures are obtained by taking advantage of the chemical etching routine. And the height of the nanogratings can be flexibly controlled through accurately restricting the duration of the etching procedure. Cross-scale structural color patterning was realized on silicon wafer surface and achieved much better surface coloring than traditional LIPSS technology. That is, highly homogeneous and controllable nanograting structures can be flexibly produced on silicon due to the regular arrangement of laser-induced amorphous-crystalline nanofringes and the exact adjustment of subsequent chemical etching operation, which would serve as a complementary method to conventional lithography methods.

2 Experimental section

2.1 Fabrication of nanograting structures

The schematic of the experimental arrangement is demonstrated in Figure 1A. The femtosecond laser directly irradiated the sample surface focused by an achromatic

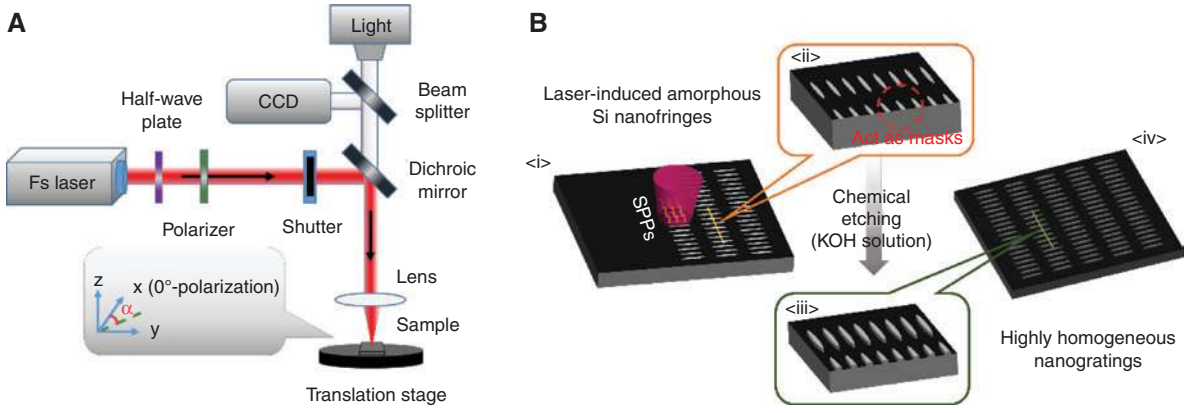

Figure 1: Schematic diagram of the experimental process.
(A) Schematic of the setup for femtosecond laser fabrication. (B) Flow chart of the chemical wet-etching assisted femtosecond laser modification approach.

doublet lens with a focal length of 100 mm. A Ti: sapphire regenerative oscillator-amplifier system (Spectra-Physics) was selected as the laser source, which provided a fundamental Gaussian laser beam with a central wavelength of 800 nm, pulse duration of 50 fs, and repetition rate of 1000 Hz. The laser fluence used in our experiments can be adjusted by controlling the half-wave plate and polarizer. Moreover, by manipulating the opening time of the mechanical shutter and the laser repetition rate, the number of pulses absorbed by the sample surface was tuned. Standard polished <100> Si wafers ($10 \times 10 \times 1$ mm) were pretreated with the HF solution to eliminate the surface oxide, followed by a 10-min ultrasonic cleaning. The processing parameters adopted in our experiments (except Figure S1) were as follows: laser fluence F = 167 mJ cm^{-2}, laser repetition rate f = 1000 Hz, and scanning speed v_{scan} = 2000 μm s^{-1}. In the subsequent chemical etching procedure, the alkaline etchant was prepared by mixing 20 mass% KOH and isopropyl alcohol in a volume ratio of 4:1, and the ambient temperature was preserved at constant 55°C. All experiments were conducted in air.

2.2 Sample characterization

The morphology of the fabricated structures was examined with a scanning electron microscope (SEM, XL30S-FEG, FEI, Inc., Hillsboro, OR, USA). An atomic force microscope (AFM, Dimension Edge PSS, Bruker, Inc., Karlsruhe, Germany) was utilized to characterize detailed topographies of the nanogratings. The material crystallographic orientation properties in the laser irradiation area were measured by Micro-Raman spectroscopy (inVia reflex, Renishaw, Gloucestershire, London, UK) employing a 532 nm laser and transmission electron microscope (TEM, JEM 2100F, JEOL Ltd., Akishima, Tokyo, JAPAN). Structural colors ranging from red to purple were captured by an ordinary camera (Canon, EOS 6D, Tokyo, Japan) with varying viewing angles, which was performed under indoor light.

3 Results and discussions

Figure 1B illustrates the schematic diagram of a flow chart of chemical wet-etching-assisted femtosecond laser modification approach. Firstly, a linearly polarized femtosecond laser beam with a central wavelength of 800 nm was scanned over the surface of the sample focused by an achromatic doublet lens with a focal length of 100 mm. As shown in Figure 1B <i>, via femtosecond laser modification, the amorphous-crystalline nanofringes were patterned on the silicon surface. Subsequently, the modified-Si wafer was etched in KOH solution for fabricating the designed structures, considering that KOH has a significantly different etching rate towards amorphous and crystalline silicon. As shown in Figure 1B <ii–iv>, the laser-induced amorphous-Si nanofringes (acting as subtle mask) gradually protruded from the surface to generate the highly homogeneous and controllable nanogratings. The details of the preparation of alkaline etchant and the ambient temperature are shown in Section 2. All experiments were conducted in air.

3.1 Processing and analysis of amorphous-silicon nanofringes

Ultrafast laser-induced melting and resolidification have been extensively studied to clarify the phase changes on silicon, that is, the amorphization of crystalline silicon and recrystallization of amorphous silicon [35–39]. In this study, we attempt to prepare amorphous silicon LIPSS (called amorphous-Si nanofringes in this paper) on crystalline silicon surface based on the SPPs surface wave excitation. As shown in Figure S1, bright nanofringes can be observed after statically irradiated by femtosecond laser pulses, using pulse number N = 5, and laser fluence F = 167 mJ cm^{-2}. The direction of the laser-induced amorphous-Si nanofringes is perpendicular to the polarization of incident laser and the average period of the nanofringes is approximately 790 ± 30 nm, which correspond to the conventional low spatial frequency LIPSS. It is commonly known that polarized pulsed laser can induce sub-wavelength periodic surface structures on the material surface. However, the interaction between the laser and the material in the generation of LIPSS is a highly complex process. Thus, the formation mechanism still remains controversial. Even so, it is now widely accepted that the interference of the incident laser field with the excitation and propagation of SPPs plays a key role in the formation of LIPSS [12]. Theoretically, although SPP is generally merely coupled and propagated on metal surfaces, it can also occur in semiconductors and dielectrics in view of the fact that semiconductors or dielectrics will be transiently turned into a metal-like state upon the femtosecond laser irradiation [40].

The modified nanofringes on Si wafer can be extended to two-dimensional by converting laser static radiation into dynamic scanning, while the laser frequency and scanning speed should be carefully controlled [41]. Figure 2A illustrates the SEM micrograph of the 2D amorphous-Si nanofringes produced by femtosecond laser scanning through the sample with laser

frequency f = 1000 Hz and scanning speed $v_{scan} = 2000$ μm s^{-1} (the effective pulse number is calculated to be $N_{eff} = 3.8$, as demonstrated in Figure S2), using the same laser fluence as Figure S1 ($F = 167$ mJ cm^{-2}). As presented in Figure 2A, the 2D alternating amorphous-crystalline nanofringes are regularly arranged on the Si wafer surface, and the black lines represent the amorphous-Si nanofringes. The period of the modified nanofringes is close to the wavelength of the incident laser ($\Lambda = 790 \pm 30$ nm) [42]. The optical microscopy image of the sample is given in the upper right inset. Bright areas featuring increased reflectivity stand for laser exposed region, and the relatively dark areas featuring different reflectivity stay unexposed.

We have measured the material crystallographic orientation characteristics of both the laser irradiated area and non-irradiated area through micro-Raman spectroscopy. Micro-Raman spectroscopy is a suitable tool for detecting the phase changing of silicon due to its high sensitivity to the crystallographic orientation of materials [12]. The red circle, blue triangle, and green square marked in Figure 2A represent the position of amorphous-Si nanofringe, crystalline-Si nanofringe, and non-irradiation zones, respectively. The resulting spectra of the corresponding detected positions in Figure 2A are illustrated in Figure 2B. As can be found in Figure 2B, the Raman spectrum of the non-irradiated area (green line) only presents the strong peak centered at 520.5 cm^{-1} which is the characteristic peak of monocrystalline silicon. In contrast, the obtained spectrum of the laser-induced nanofringe (red line in Figure 2B) possesses a broad band centered at 473 cm^{-1}, which symbolizes the existence of amorphous silicon. Since the detecting depth of the micro-Raman spectroscopy is much larger than the thickness of the modified region, the Raman signal of the monocrystalline silicon substrate can be efficiently collected. Hence, the Raman spectrum of the amorphous-Si nanofringes exhibits a strong peak at 520.5 cm^{-1} as well. We have also taken the region between two amorphous-Si nanofringes (the position marked by the blue triangle in Figure 2A) into consideration. The consequent spectrum only shows the characteristic peak of monocrystalline silicon.

A TEM test has also been performed to investigate the changing in the material property of the laser irradiated region. Figure 2C and D show the cross-sectional TEM images of the laser-modified area before chemical

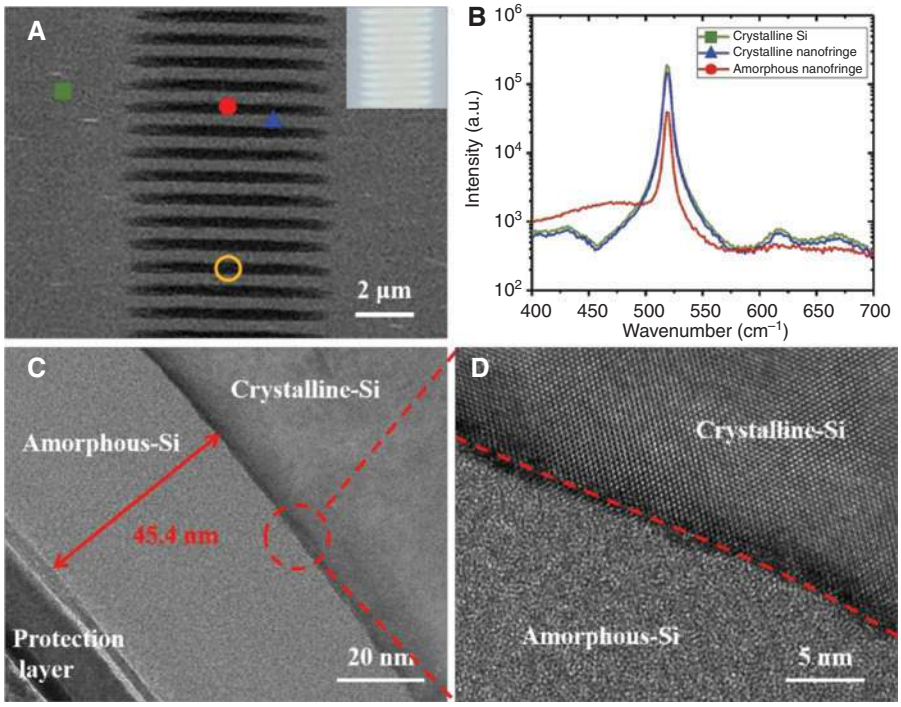

Figure 2: Processing and analysis of amorphous-silicon nanofringes.
(A) SEM micrograph of the modified nanofringes on Si wafer produced by femtosecond laser scanning through the sample with a constant velocity $v_{scan} = 2000$ μm s^{-1}, using laser fluence $F = 167$ mJ cm^{-2}. (B) Raman spectra corresponding to the marked positions in (A). The red circle, blue triangle, and green square marked in (A) represent the position of amorphous-Si nanofringe, crystalline-Si nanofringe, and non-irradiation zones, respectively. The colors of the Raman spectra in (B) correspond to the marks in (A). (C) TEM image of the laser-modified region marked by a yellow circle in (A). (D) A partial enlarged view of (C).

etching. The test sample was obtained from the position marked by the yellow circle in Figure 2A. As demonstrated in Figure 2C, an obvious boundary between the laser-modified shallow layer and the monocrystalline silicon substrate can be observed. Moreover, the high-resolution TEM image in Figure 2D clearly illustrates the changing in the crystallographic orientation of the monocrystalline silicon after laser irradiation. Atoms are in disordered arrangement in the laser-modified layer (the lower left part of Figure 2D), which is the characteristic feature of amorphous silicon, while the laser-unexposed substrate portion remains highly ordered (the upper right part of Figure 2D), implying the intrinsic nature of monocrystalline silicon. As expected, the laser-induced structure shown in Figure 2A is indeed the alternating amorphous-crystalline silicon nanofringes. The layer of the laser-induced amorphous Si is about 45.4 nm thick in this paper (as illustrated in Figure 2C), which corresponds well to the fabricated results by Izawa et al. [43].

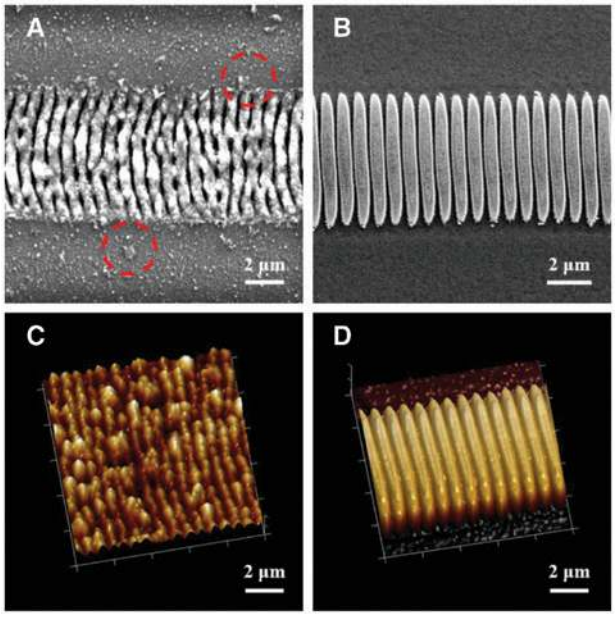

Figure 3: Homogeneity comparison of the fabricated structures. (A) SEM micrograph of the conventional LIPSSs fabricated by using laser scanning speed $v_{scan} = 1000$ μm s^{-1} and laser fluence F = 450 mJ cm^{-2}. (B) SEM micrograph of nanograting structures fabricated by chemical etching assisted femtosecond laser modification, using scanning speed $v_{scan} = 2000$ μm s^{-1}, laser fluence F = 167 mJ cm^{-2}, and etching time $T_{et} = 60$ s. (C) and (D) AFM images show the details of the surface morphology of (A) and (B).

3.2 Fabrication of nanogratings with high homogeneity and controllability

Nonhomogeneity has always been one of the main factors that hinder the widespread use of LIPSS. In the processing of traditional LIPSS, a relatively high laser fluence is utilized to bring forth local ablation of the material aiming at forming the grating structures. Laser-induced material ablation is always accompanied by the production of plenty of debris and surface defects, which will critically affect the propagation of SPPs and the subsequent distribution of light fields, leading to the nonhomogeneity of the fabricated structures. As shown in Figure 3A, rough pits in silicon are observed near the edge, and a majority of debris and recast layers are attached to the grating structures fabricated in a conventional pathway. On the contrary, the nanogratings fabricated in our experiment are highly homogeneous, which is generated in the following two steps: (i) amorphous-crystalline Si nanofringes are generated by focused femtosecond laser scanning through the silicon wafer surface, adopting constant scanning speed $v_{scan} = 2000$ μm s^{-1} and laser fluence F = 167 mJ cm^{-2} that are the same as in Figure 2A; (ii) the laser-modified sample is then placed in a KOH solution for chemical etching during which the laser-induced amorphous-Si acts as a subtle mask to prepare the designed structures, because the etching rate of the amorphous-Si in KOH solution is much slower than that of the crystalline Si. As shown in Figure 3B, the nanogratings fabricated by our technology possess high uniformity, and each grating distributes independently with no visible bifurcations (in Figure 3B, the etching time was 60 s). In addition, energy-dispersive X-ray analyses are performed in the laser exposed area and the laser unexposed area. As illustrated in Figure S3, there are no traces of oxygen in both regions, thereby eliminating the effect of the presence of surface oxygen on the etched topography. Hence, the regular arrangement of the laser-induced amorphous-Si nanofringes and the further chemical treatment would contribute to the great homogeneity. There are many factors affecting the etching rate of silicon in the alkaline solution (KOH), such as ambient temperature, solution concentration, etc., while the etching rate is also critically related to the dangling bond density and energy level of silicon [44, 45]. Under the same condition of constant concentration of alkaline solution and ambient temperature, the etching rate of (100) crystalline Si is nearly 30 times higher than that of amorphous Si, which is mainly attributed to the higher average dangling bond density and back bond energy level of the silicon atoms on crystalline Si [45–48]. During the chemical etching, the (100) crystalline Si exposed to etching solution is quickly removed, while the laser-induced amorphous-Si nanofringes gradually protrude to form the nanogratings.

To completely characterize the morphology of the traditional LIPSS and the nanograting structures fabricated by chemical etching-assisted femtosecond laser modification, we performed AFM analysis on both structures. The measured results are demonstrated in Figure 3C (traditional LIPSS) and Figure 3D (nanograting structures), respectively. Obviously, the nanograting structures fabricated by our technology (Figure 3D) are regularly distributed, closely aligned, and highly homogeneous compared with traditional LIPSS (Figure 3C).

However, the formation of regularly arranged nanogratings is critically sensitive to laser parameters. As demonstrated in Figure 4B, a weakly ablated area appears at the center of the nanofringes, while the effective pulses number is slightly increased from $N_{eff}=3.8$ (Figure 4A, using $v_{scan}=2000\ \mu m\ s^{-1}$) to $N_{eff}=5.1$ (Figure 4B, using $v_{scan}=1500\ \mu m\ s^{-1}$). Besides, when the effective pulses number is reduced to $N_{eff}=1.9$ (Figure 4C, using $v_{scan}=4000\ \mu m\ s^{-1}$), only several separate modified points are obtained. The laser fluence adopted in the above three cases is constant ($F=167\ mJ\ cm^{-2}$). In addition to the effective pulses number, laser fluence also has dramatic influence on the amorphous nanofringes formation. In Figure 4D, as the laser fluence is set to 210 mJ cm^{-2} (slightly higher than in Figure 4A) and the scanning speed is fixed at 2000 μm s^{-1}, a micro-scale modified line is generated in the laser-irradiated region rather than mutually independent nanofringes. The corresponding etched structures are illustrated in the SEM micrographs in Figure 4A–D. It's clearly observed that only ordered laser-modified nanofringes, prepared at certain laser parameters, can be transformed into highly uniform nanograting structures during the subsequent chemical etching process. Notably, as demonstrated in Figure S4, large-area continuous nanogratings are successfully fabricated by precisely selecting the laser scanning interval (7 μm in our experiments) when applying our technology.

Morphology controllability is a crucial characteristic of nanofabrication technique. Thus, in the following section, we are about to demonstrate the controllability of the nanogratings fabricated by chemical etching-assisted femtosecond laser modification approach. Namely, varying the chemical etching time enables flexible tuning of the height of the nanograting structures. Figure 5A–D show the SEM micrographs (left) and 3D AFM images (right) of different acquired nanograting structures while laser fluence and scanning rate remained constant ($F=167\ mJ\ cm^{-2}$ and $v_{scan}=2000\ \mu m\ s^{-1}$), but various etching time of 60 s, 90 s, 120 s, and 180 s were set, respectively. It is worthy to note that the heights of the structures increase by degrees from Figure 5A–D and are significantly higher than the

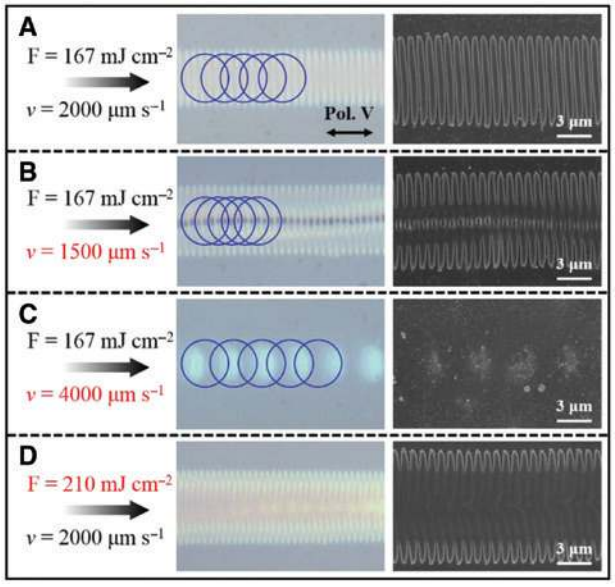

Figure 4: Morphology dependence of nanogratings on femtosecond laser parameters.
The optical images in (A–D) are the laser-induced regions based on different laser parameters. The SEM micrographs in (A–D) are the corresponding etched results with etching duration of 90 s in KOH solution. The scales used in (A–D) are 3 μm.

laser-induced amorphous-Si nanofringes (Figure 2A). We measured the average heights and averages widths of the nanogratings demonstrated in Figure 5A–D. The statistical data in Figure 5E lead us to the conclusion that the average height of the nanogratings varies almost linearly over the etching time (the average heights in Figure 5A–D are as follows: 92±5 nm, 130±5 nm, 191±5 nm, and 256±5 nm). The inserts are the corresponding cross-section images of these four kinds of nanogratings, which clearly illustrate the height and shape of the gratings. That is to say that the height of the gratings can be precisely controlled by imposing limitations on the duration of the etching process. The length of the nanograting structure depends on the length of the laser-induced amorphous-Si nanofringe. Similar to the elapse of etching time, the average width of the grating structures undergoes a slight decrease. As shown in the right column of Figure 5E, the mean width values are 7.2±0.5 μm, 7.1±0.5 μm, 7.0±0.5 μm, and 6.7±0.5 μm, respectively).

3.3 Structural color display

Periodic surface structures which possess the quality of behaving as diffractive grating to generate structural color present a promising application prospect in the field of sample-based surface coloring. Similar to butterfly wings, when light irradiates the large-area nanograting

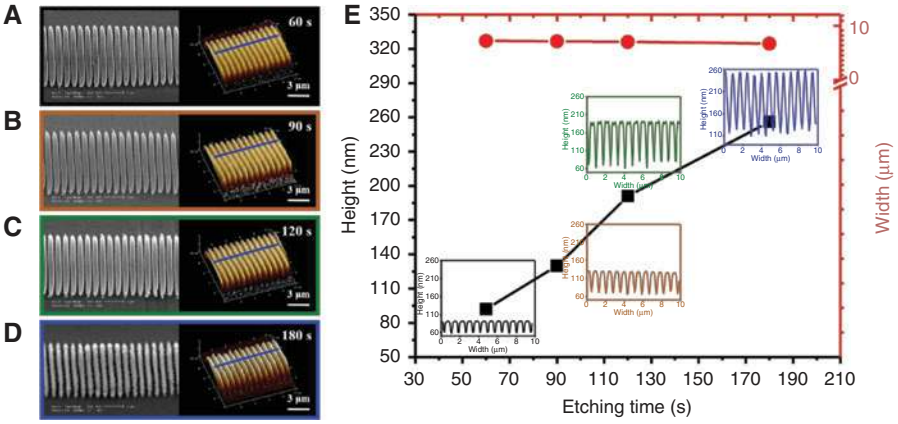

Figure 5: Morphology controllability of the nanograting structures.
(A–D) SEM micrographs (left) and AFM images (right) of the nanogratings by different etching processes (etching for 60 s, 90 s, 120 s, and 180 s, respectively). (E) Topography dependence of silicon nanograting structures on etching time. The inserts are the corresponding cross-section images.

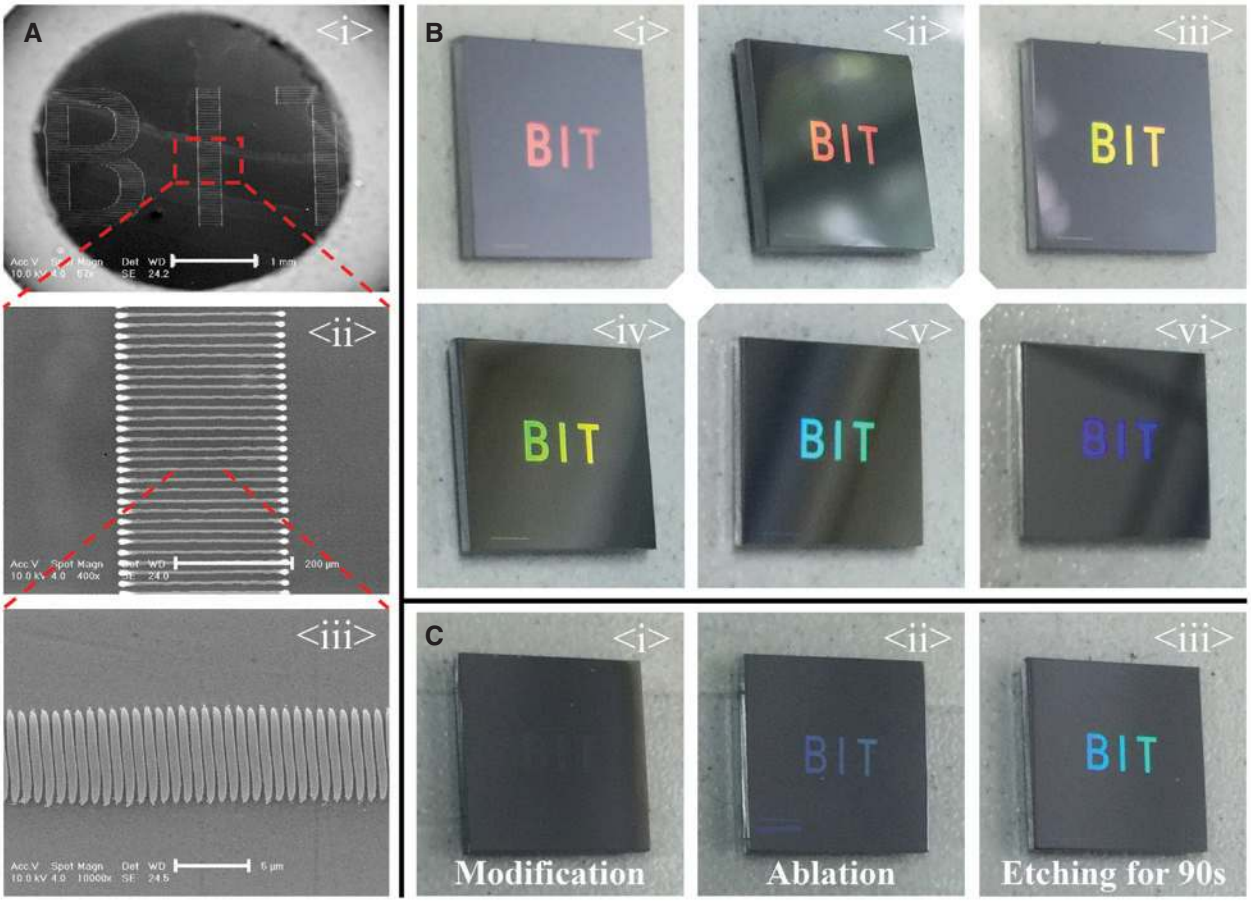

Figure 6: "BIT"-shaped large-area nanograting structures fabricated by chemical etching-assisted femtosecond laser modification, using $F = 167$ mJ cm^{-2}, $v_{scan} = 2000$ μm s^{-1}, and $T_{et} = 90$ s, respectively.
(A) SEM micrographs of the fabricated structure. (A <ii>) and (A <iii>) are the magnified depictions of (A <i>). The scales in (A) are 1 mm, 200 μm, and 5 μm, respectively. (B) The structural colors of the Si surface with 2D nanograting structures. Gradual changing of the viewing angle leads to the appearance of color red to purple shade due to the chromatic dispersion. (C) The structural colors of the Si surface adopting three different processing methods. A detailed comparison of the structural colors is shown in Videos S1–S3.

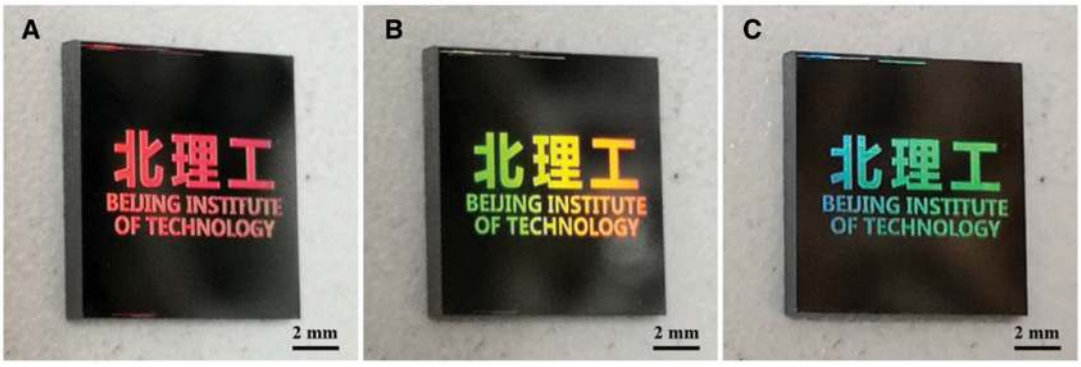

Figure 7: A Si surface with complex patterned graphics made up of 2D nanograting structures with cross scales from 790 nm to 0.75 cm. (A–C) The structural colors of the Si surface are observed from different angles captured by an ordinary camera under indoor illumination.

structures, structural color can be clearly observed [49]. According to Figure 6B, diverse colors throughout the visible spectrum are obtained via varying the incident light angle and viewing angle. This appearance is summarized as the diffraction grating equation shown in Equation (1):

$$\mathbf{m}\lambda = \mathbf{d}(\sin\theta_D - \sin\theta_I), \tag{1}$$

where **m** is the diffraction order, **d** is the period of the nanogratings (in this paper, **d** = 790nm), and θ_I and θ_D represent the incident light angle and the diffraction angle, respectively [50]. Figure 6A shows the large "BIT"-shaped nanograting structures fabricated by the aforementioned method wherein chemical etching was employed for 90 s. Enlarged views of Figure 6A <i> are given in Figure 6A <ii> and <iii>. Figure 6B demonstrates the iridescence of Figure 6A captured by the camera when illuminating the structures with a beam of sunlight source. Keeping the angle of incident light unaltered, the light of different wavelengths is diffracted from corresponding diffraction angles. It is apparent from Figure 6B <i–vi> that while the viewing angle is gradually changed, various colors from red to purple are spotted.

Besides, the comparison of the structural colors of the surface structures generated by three different processing methods is performed in Figure 6C. Figure 6C <i> illustrates the fabrication of femtosecond laser-modified amorphous-crystalline structures without the subsequent etching process. The nanograting structures of Figure 6C <ii> were produced by conventional LIPSS method. Figure 6C <iii> pictures the nanograting structures fabricated by the approach mentioned above, noting that the chemical etching lasted for 90 s. The nanograting structures created by chemical etching-assisted femtosecond laser modification exhibit more favorable structural color characteristics, which is consistent with the spectroscopy measurements in Figure S5. This is attributed to the high homogeneity and controllable height of the nanograting structures induced by our method.

Moreover, the structural colors of the Si surface with complex patterned design are depicted in Figure 7, which are made up of 2D nanograting structures with cross scales from 790 nm to 0.75 cm. It is noteworthy that these 2D nanograting structures were fabricated by chemical etching-assisted femtosecond laser modification with etching for 90 s. This design is composed of the Chinese abbreviation and English full text of "Beijing Institute of Technology". Figure 7A–C have displayed three different kinds of structural color viewing from several angles only under indoor light illumination (as shown in Video S4). These well-defined patterns will undoubtedly confirm that our approach is capable of producing any desirable pattern with remarkable structural color characteristics.

4 Conclusion

In summary, a flexible and efficient approach has been proposed to fabricate highly homogeneous and controllable nanograting structures on a silicon surface via chemical etching-assisted femtosecond laser modification. In the first stage, high-precision alternating amorphous-crystalline nanofringes are generated on a Si wafer due to femtosecond laser interaction with monocrystalline silicon. Subsequently, assisted by chemical etching, extremely homogeneous nanograting structures are acquired resulting from the distinct etching rates of amorphous silicon and crystalline silicon in KOH solution. Besides, the morphology of the nanogratings can be precisely controlled by simply adjusting the etching process. Afterwards, the structural

color of the Si surface featuring 2D nanograting structures is investigated. When varying the viewing angle, the colors of the visible spectrum from red to purple are observed on account of the chromatic dispersion. Meanwhile, the consequent nanograting structures exhibit more favorable structural color properties. Furthermore, this approach holds tremendous potentiality to create any complex pattern with remarkable structural color characteristics on silicon. This flexible and efficient processing strategy for fabricating nanogratings with high homogeneity facilitates applications in broad fields, such as optics, biotechnology, etc.

Acknowledgments: This work is financially supported by the National Key R&D Program of China (No. 2018 YFB1107200), National Natural Science Foundation of China (NSFC) (No. 51675049 and No. 51675048), Natural Science Foundation of Beijing Municipality (No. 3172027), and Young Elite Scientists Sponsorship Program (No. 2016QNRC001).

Competing financial interests: The authors declare no competing financial interests.

References

[1] Schanze KS, Bergstedt TS, Hauser BT. Photolithographic patterning of electroactive polymer films and electrochemically modulated optical diffraction gratings. Adv Mater 1996;8:531–4.
[2] Butt H, Montelongo Y, Butler T, et al. Carbon nanotube based high resolution holograms. Adv Mater 2012;24: OP331–6.
[3] Montelongo Y, Tenoriopearl JO, Milne WI, et al. Polarization switchable diffraction based on subwavelength plasmonic nanoantennas. Nano Lett 2014;14:294.
[4] Marshall OP, Chakraborty S, Khairuzzaman M, et al. Reversible mode switching in Y coupled terahertz lasers. Appl Phys Lett 2013;102:111105.
[5] Zhao Q, Yetisen AK, Anthony CJ, et al. Printable ink holograms. Appl Phys Lett 2015;107:041115.
[6] Birnbaum M. Semiconductor surface damage produced by ruby lasers. J Appl Phys 1965;36:3688–9.
[7] Driel HMV, Sipe JE, Young JF. Laser-induced periodic surface structure on solids: a universal phenomenon. Phys Rev Lett 1982;49:1955–8.
[8] Sipe JE, Young JF, Preston JS, et al. Laser-induced periodic surface structure. I. Theory. Phys Rev B 1983;27:1141–54.
[9] Bonse J, Munz M, Sturm H. Structure formation on the surface of indium phosphide irradiated by femtosecond laser pulses. J Appl Phys 2005;97:013538.
[10] Yuan Y, Jiang L, Li X, et al. Formation mechanisms of subwavelength ripples during femtosecond laser pulse train processing of dielectrics. J Phys D Appl Phys 2012;45:175301–6.
[11] Han W, Jiang L, Li X, et al. Continuous modulations of femtosecond laser-induced periodic surface structures and scanned line-widths on silicon by polarization changes. Opt Express 2013;21:15505–13.
[12] Bonse J, Krüger J. Pulse number dependence of laser-induced periodic surface structures for femtosecond laser irradiation of silicon. J Appl Phys 2010;108:034903.
[13] Vorobyev AY, Guo C. Colorizing metals with femtosecond laser pulses. Appl Phys Lett 2008;92:041914.
[14] Dusser B, Sagan Z, Soder H, et al. Controlled nanostructrures formation by ultra fast laser pulses for color marking. Opt Express 2010;18:2913–24.
[15] Li J, Ho S, Haque M, et al. Nanograting Bragg responses of femtosecond laser written optical waveguides in fused silica glass. Opt Mater Express 2012;2:1562–70.
[16] Yuan H-C, Yost VE, Page MR, et al. Efficient black silicon solar cell with a density-graded nanoporous surface: optical properties, performance limitations, and design rules. App Phys Lett 2009;95:123501.
[17] Zorba V, Stratakis E, Barberoglou M, et al. Biomimetic artificial surfaces quantitatively reproduce the water repellency of a lotus leaf. Adv Mater 2008;20:4049–54.
[18] Martín-Fabiani I, Rebollar E, Pérez S, et al. Laser-induced periodic surface structures nanofabricated on poly (trimethylene terephthalate) spin-coated films. Langmuir 2012;28:7938–45.
[19] Drakakis TS, Papadakis G, Sambani K, et al. Construction of three-dimensional biomolecule structures employing femtosecond lasers. Appl Phys Lett 2006;89:144108.
[20] Jiang L, Ying D, Li X, et al. Two-step femtosecond laser pulse train fabrication of nanostructured substrates for highly surface-enhanced Raman scattering. Opt Lett 2012;37:3648–50.
[21] Liu XQ, Chen QD, Guan KM, et al. Dry-etching-assisted femtosecond laser machining. Laser Photonics Rev 2017;11:1600115.
[22] Bucksbaum PH, Bokor J. Rapid melting and regrowth velocities in silicon heated by ultraviolet picosecond laser pulses. Phys Rev Lett 1984;53:182–5.
[23] Shumay I, LHöfer U. Phase transformations of an InSb surface induced by strong femtosecond laser pulses. Phys Rev B Condens Matter 1996;53:15878–84.
[24] Garcia-Lechuga M, Puerto D, Fuentes-Edfuf Y, et al. Ultrafast moving-spot microscopy: birth and growth of laser-induced periodic surface structures. ACS Photonics 2016;3:1961–7.
[25] Puerto D, Garcia-Lechuga M, Hernandez-Rueda J, et al. Femtosecond laser-controlled self-assembly of amorphous-crystalline nanogratings in silicon. Nanotechnology 2016;27:265602.
[26] Li X, Xie Q, Jiang L, et al. Controllable Si (100) micro/nanostructures by chemical-etching-assisted femtosecond laser single-pulse irradiation. Appl Phys Lett 2017;110:181907.
[27] Taylor R, Hnatovsky C, Simova E. Applications of femtosecond laser induced self-organized planar nanocracks inside fused silica glass. Laser Photonics Rev 2008;2:26–46.
[28] Sivakov V, Andrä G, Gawlik A, et al. Silicon nanowire-based solar cells on glass: synthesis, optical properties, and cell parameters. Nano Lett 2009;9:1549–54.
[29] Fan FR, Lin L, Zhu G, et al. Transparent triboelectric nanogenerators and self-powered pressure sensors based on micropatterned plastic films. Nano Lett 2012;12:3109.
[30] Meng B, Tang W, Too Z, et al. A transparent single-friction-surface triboelectric generator and self-powered touch sensor. Energ Environ Sci 2013;6:3235–40.

[31] Osellame R, Hoekstra HJ, Cerullo G, et al. Femtosecond laser microstructuring: an enabling tool for optofluidic lab-on-chips. Laser Photonics Rev 2011;5:442–63.
[32] Sugioka K, Hanada Y, Midorikawa K. Three-dimensional femtosecond laser micromachining of photosensitive glass for biomicrochips. Laser Photonics Rev 2010;4:386–400.
[33] Deng Z, Yang Q, Chen F, et al. Fabrication of large-area concave microlens array on silicon by femtosecond laser micromachining. Opt Lett 2015;40:1928–31.
[34] Canavese G, Marasso SL, Quaglio M, et al. Polymeric mask protection for alternative KOH silicon wet etching. J Micromech Microeng 2007;17:1387.
[35] Thompson MO, Galvin G, Mayer J, et al. Melting temperature and explosive crystallization of amorphous silicon during pulsed laser irradiation. Phys Rev Lett 1984;52:2360.
[36] Liu P, Yen R, Bloembergen N, et al. Picosecond laser-induced melting and resolidification morphology on Si. Appl Phys Lett 1979;34:864–6.
[37] Tsu R, Hodgson RT, Tan TY, et al. Order-disorder transition in single-crystal silicon induced by pulsed UV laser irradiation. Phys Rev Lett 1979;42:1356.
[38] Cullis A, Webber H, Chew N, et al. Transitions to defective crystal and the amorphous state induced in elemental Si by laser quenching. Phys Rev Lett 1982;49:219.
[39] Thompson MO, Mayer J, Cullis A, et al. Silicon melt, regrowth, and amorphization velocities during pulsed laser irradiation. Phys Rev Lett 1983;50:896.
[40] Huang M, Zhao F, Cheng Y, et al. Origin of laser-induced near-subwavelength ripples: interference between surface plasmons and incident laser. ACS Nano 2009;3:4062–70.
[41] Fuentes-Edfuf Y, Garcia-Lechuga M, Puerto D, et al. Coherent scatter-controlled phase-change grating structures in silicon using femtosecond laser pulses. Sci Rep 2017;7:4594.
[42] Bonse J, Rosenfeld A, Krüger J. On the role of surface plasmon polaritons in the formation of laser-induced periodic surface structures upon irradiation of silicon by femtosecond-laser pulses. J Appl Phys 2009;106:104910.
[43] Izawa Y, Izawa Y, Setsuhara Y, et al. Ultrathin amorphous Si layer formation by femtosecond laser pulse irradiation. Appl Phys Lett 2007;90:044107.
[44] Seidel H, Csepregi L, Heuberger A, et al. Anisotropic etching of crystalline silicon in alkaline solutions I. Orientation dependence and behavior of passivation layers. J Electrochem Soc 1990;137:3612–26.
[45] Monteiro TS, Kastytis P, Gonçalves LM, et al. Dynamic wet etching of silicon through isopropanol alcohol evaporation. Micromachines 2015;6:1534–45.
[46] Wan Y, Yan D, Bullock J, et al. Passivation of c-Si surfaces by sub-nm amorphous silicon capped with silicon nitride. Appl Phys Lett 2015;107:231606.
[47] Kawasegi N, Morita N, Yamada S, et al. Etch stop of silicon surface induced by tribo-nanolithography. Nanotechnology 2005;16:1411.
[48] Park JW, Kawasegi N, Morita N, et al. Mechanical approach to nanomachining of silicon using oxide characteristics based on tribo nanolithography (TNL) in KOH solution. J Manuf Sci Eng 2004;126:801–6.
[49] Sato O, Kubo S, Gu Z-Z. Structural color films with lotus effects, superhydrophilicity, and tunable stop-bands. Accounts Chem Res 2008;42:1–10.
[50] Yao J, Zhang C, Liu H, et al. Selective appearance of several laser-induced periodic surface structure patterns on a metal surface using structural colors produced by femtosecond laser pulses. Appl Surf Sci 2012;258:7625–32.

Supplementary Material: The online version of this article offers supplementary material (https://doi.org/10.1515/nanoph-2019-0056).